


# Graphene oxide-ellagic acid nanocomposite as effective anticancer and antimicrobial agent

Samer Hasan Hussein-Al-Ali<sup>1,2</sup>  | Suha Mujahed Abudoleh<sup>2</sup> | Mohd Zobir Hussein<sup>3</sup> | Saifullah Bullo<sup>3</sup> | Arul Palanisamy<sup>4</sup>

<sup>1</sup>Department of Chemistry, Faculty of Science, Isra University, Amman, Jordan

<sup>2</sup>Faculty of Pharmacy, Isra University, Amman, Jordan

<sup>3</sup>Materials Synthesis and Characterization Laboratory, Institute of Advanced Technology (ITMA), University Putra Malaysia, Selangor, Malaysia

<sup>4</sup>Laboratory of Vaccines and Immunotherapeutics, Institute of Bioscience, University Putra Malaysia, Selangor, Malaysia

## Correspondence

Samer Hasan Hussein-Al-Ali, Department of Chemistry, Faculty of Science, Isra University, P.O. Box 22, Amman 11622, Jordan.  
Email: [samer.alali72@yahoo.com](mailto:samer.alali72@yahoo.com); [samer.alali@iu.edu.jo](mailto:samer.alali@iu.edu.jo)

## Funding information

University Putra Malaysia, Grant/Award Number: 94431004; Isra University

## Abstract

In this study, ellagic acid (ELA), a skin anticancer drug, is capped on the surface(s) of functionalised graphene oxide (GO) nano-sheets through electrostatic and  $\pi$ - $\pi$  stacking interactions. The prepared ELA-GO nanocomposite have been thoroughly characterised by using eight techniques: Fourier-transform infrared spectroscopy (FTIR), zeta potential, X-ray diffraction (XRD), thermogravimetric analysis (TGA), Raman spectroscopy, atomic force microscopy (AFM) topographic imaging, transmission electron microscopy (TEM), and surface morphology via scanning electron microscopy (SEM). Furthermore, ELA drug loading and release behaviours from ELA-GO nanocomposite were studied. The ELA-GO nanocomposite has a uniform size distribution averaging 88 nm and high drug loading capacity of 30 wt.%. The in vitro drug release behaviour of ELA from the nanocomposite was investigated by UV-Vis spectrometry at a wavelength of  $\lambda_{\max}$  257 nm. The data confirmed prolonged ELA release over 5000 min at physiological pH (7.4). Finally, the  $IC_{50}$  of this ELA-GO nanocomposite was found to be 6.16  $\mu\text{g}/\text{ml}$  against B16 cell line; ELA and GO did not show any cytotoxic effects up to 50  $\mu\text{g}/\text{ml}$  on the same cell lines.

## 1 | INTRODUCTION

Ellagic acid (ELA) is an organic hetero-tetra-cyclic compound with planar phenolic lactone properties. It is found in many fruits and vegetables, such as pomegranates, cranberries, strawberries and raspberries. It has a role as a natural phenol antioxidant, which is a group of anticancer drugs [1,2]. ELA is usually inserted into drug delivery vehicles including zinc layered hydroxides [3], silver nanoparticles [4], metalla-cages [5], polylactide glycolide (PLGA) nanoparticles [6], and chitosan nanoparticles [7].

Development of research on nanomaterials for medical applications has been carried out in the last three decades; most researches concentrated on their safety and toxicity on human cell and tissue function [8–11]. However, the biomedical applications of GO, such as anticancer drug delivery,

developed quickly over the past 15 years. Graphene oxide (GO) has been extensively researched as a promising bio-carbon-material for different medical applications due to their exclusive properties: two-dimensional planar structure with  $sp^2$  hybridised carbon, large surface area with different functional groups (hydroxyl, carboxylic groups and epoxide) [12], chemical stability and excellent biocompatibility. These properties lead to exclusive applications for drug delivery systems [13,14]. Recently, different attempts have been made to incorporate different compounds for the preparation of soluble graphene for drug delivery such as the incorporation of 1-amino-octadecane [15], isocyanatobenzene [16], 5-(4-aminophenyl)-10,15,20-(triphenyl)porphyrin [17], doxorubicin hydrochloride [18], and docetaxel [19].

In this present study, the anticancer drug ELA was chosen as a model using modified GO. These new nanocomposite

This is an open access article under the terms of the Creative Commons Attribution License, which permits use, distribution and reproduction in any medium, provided the original work is properly cited.

© 2021 The Authors. *IET Nanobiotechnology* published by John Wiley & Sons Ltd on behalf of The Institution of Engineering and Technology.

were characterised and applied on B16 cancer cell lines and different microorganisms to check their drug activity.

## 2 | MATERIALS

Graphite (Gr), ELA (97% purity), phosphate-buffered saline (PBS) and modified Dulbecco's medium (DMEM) were purchased from Sigma-Aldrich (St Louis, MO, USA); potassium permanganate ( $\text{KMnO}_4$ , 99%), sulphuric acid ( $\text{H}_2\text{SO}_4$ , 95%–97%), diethyl ether ( $\text{C}_2\text{H}_5)_2\text{O}$ , hydrochloric acid (HCl, 37%), hydrogen peroxide ( $\text{H}_2\text{O}_2$ , 35%), and o-phosphoric acid ( $\text{H}_3\text{PO}_4$ , 85%) were obtained from [Friendemann.Schmidt](#). The Cell Counting Kit-8 (CCK-8) used was manufactured by Dojindo Lab (Japan), and the 96-well microplates were purchased from Corning Technologies (Corning, NY, USA).

The bacterial strains used were obtained from the Faculty of Medicine at the University of Jordan (Jordan). The bacterial strains studied are *Proteus mirabilis* (ATCC12453), methicillin-resistant *Staphylococcus aureus* (MRSA) (ATCC43300), *Pseudomonas aeruginosa* (ATCC27853), *Klebsiella pneumoniae* (ATCC13883), *Escherichia coli* (ATCC8739) and *Staphylococcus aureus* (ATCC33862).

## 3 | METHODS

### 3.1 | Convert graphite to graphene oxide

Graphite (Gr) was converted to GO using a modified Hummers method [20]. The stepwise preparation is as follows:

1. The Gr flakes (3 mg) and  $\text{KMnO}_4$  (38 g) were mixed in 360 ml of  $\text{H}_2\text{SO}_4$  (98%) and 40 ml of  $\text{H}_3\text{PO}_4$  in a 1000 ml-volumetric flask and kept in an ice bath.
2. The mixture was stirred continuously for 12 h with heating at 50 C and then cooled to room temperature.
3. The content of the reaction was poured into 400 ml ice and 3 ml  $\text{H}_2\text{O}_2$  (30%), and centrifuged at 4000 rpm for 3 min. The washing was carried out using water, 200 ml HCl (37%) and 200 ml ethanol.
4. The coagulation process occurred using 200 ml diethyl ether.
5. Finally, the GO was filtered by Ommipore membrane.

### 3.2 | Preparation of the ellagic acid-graphene oxide nanocomposite

The ELA-GO nanocomposite were prepared as follows: 0.3410 g of ELA was dissolved in 50 ml of dimethyl sulfoxide (DMSO), stirred and heated up to 40°C. After that, 0.2 g of GO were mixed with the ELA solution, and the pH was adjusted to 4.7 using NaOH. The reaction contents were stirred for 18 h. The final product was filtered and washed with deionised water five times; the nanocomposite was dried in an oven for 12 h.

### 3.3 | Loading of ellagic acid into and release from ellagic acid-graphene oxide nanocomposite

The amount of ELA loaded into the ELA-GO nanocomposite was determined by separating the ELA solution from GO. Different terms are used during the calculation;  $T_i$  is the initial mass of drug used in the experiment,  $T_f$  is the mass of drug in supernatant. Therefore  $T_i - T_f$  represents the mass of drug binding in the formulation.

The procedure for determination of  $T_f$  was carried out by centrifuge the nanocomposite at 4000 rpm for 10 min and the absorbance was measured. The mass of unbinding ELA in the supernatant was measured through the calibration curve.

The mass of the nanocomposite was determined after the centrifugation, washing and drying the formulation. All the previous steps were measured by a UV spectrophotometer at a wavelength of 257 nm and used in the following Equation (1):

$$\text{Loading Efficiency}\% = \frac{T_i - T_f}{\text{mass of nanocomposite}} \times 100 \quad (1)$$

The ELA release from ELA-GO nanocomposite was determined by using a PBS solution similar to physiological body pH (pH 7.4). About 100 mg of the ELA-GO nanocomposite was added to 500 ml of PBS. About 2 ml from release medium was removed at different times and exchanged with 2 ml of the buffer. The cumulative amount of ELA free in the solution was measured at  $\lambda_{\text{max}} = 257$  nm using a Shimadzu UV-1601 spectrophotometer instrument. To compare the release behaviour of ELA from ELA-GO with that from the physical form, the 30 mg of ELA was mixed with 70 mg of GO and determined by a phosphate-buffered solution.

### 3.4 | Cell culturing and cytotoxicity assays

The CCK-8 assay was used to measure the cell viability in a microplate reader. The B16-F10 and 3T3 cell lines were harvested in 96-multi-well plates at a cell density of  $1.5 \times 10^5$  cells/ml in 100  $\mu\text{l}$  of Roswell Park Memorial Institute (RPMI) 1640 medium which contained DMEM supplemented with 10% heat-inactivated fetal bovine serum (FBS). The old media was removed, and then, 100  $\mu\text{l}$  of the new DMEM medium containing ELA, GO, and ELA-GO nanocomposite was used to treat the B16-F10 and 3T3 cells. The control wells contained only media and cells. A 10  $\mu\text{l}$  sample of CCK-8 assay was added to the wells under conditions of 37°C in a 5% carbon dioxide humidified incubator. The absorbance of each well was measured using a microplate reader at  $\lambda_{\text{max}} = 450$  nm. The cell viability was calculated according to the literature [21].

### 3.5 | Test material preparations for microorganisms

The ELA was dissolved in DMSO to final concentrations of 5, 1 and 0.5 mg/ml. The suspension of GO was prepared in 0.9% PBS into a final concentration of 5 mg/ml. The ELA-GO nanocomposite was prepared as a suspension in 0.9% normal saline into final concentrations of 5, 1, and 0.5 mg/ml. The DMSO alone was used as a negative control.

### 3.6 | Antibacterial assay

The antibacterial activity of ELA-GO nanocomposite was evaluated by the agar well diffusion method using nutrient agar medium for the assay. The microorganism under study was activated by inoculating a loopful of the strain in 10 ml of the nutrient broth and incubated at 37 C in an orbital shaker. The density of each of the bacterial strains was adjusted to 0.5 McFarland. 100  $\mu$ l of each McFarland was spread over the surface of nutrient agar. After that, a well was made in the seeded plates with the help of an 8 mm cup-borer. 100  $\mu$ l of the test materials was introduced into the wells, followed by incubation at 37 C for 24 h. The antibacterial activity was tested in triplicates by measuring the diameter of the zone of inhibition.

## 4 | INSTRUMENTATION

All the prepared samples were measured using different instruments described as follows:

1. Powder X-ray diffraction (PXRD) in the range of 2°–40° by 6000 diffractometer model (Shimadzu, Tokyo, Japan) with CuK ( $\alpha$ ) X-ray sources ( $\lambda$  1.54 Å) at 30 kV and 30 mA.
2. Fourier-transform infrared spectroscopy (FTIR) data spectra of the ELA, GO and ELA-GO nanocomposites were measured in the range of 400–4000  $\text{cm}^{-1}$  wave number on a Thermo Nicolet Nexus, Smart Orbit spectrometer.
3. TGA was conducted using a Mettler-Toledo 851e instrument (Switzerland) at a heating rate of 10°C/min from 30° C to 900°C.
4. Transmission electron microscope imaging of the GO and ELA-GO nanocomposites were studied using FEI model (USA).
5. Raman imaging spectra were measured using a UHTS 300 model (WITec, Germany) with excitation at 532 nm.
6. The zeta potential ( $\zeta$ ) was determined at room temperature by dynamic light scattering using a Malvern Zetasizer Nano ZS instrument (United Kingdom).
7. The ultraviolet–visible (UV–Vis) spectra were measured to determine the controlled release study, using a UV–Vis spectrophotometer (Shimadzu UV-1601).

## 5 | RESULTS OF THE DATA AND DISCUSSION

### 5.1 | Powder X-ray diffraction

Figure 1a–d shows the PXRD patterns of Gr, GO, ELA-GO nanocomposite and ELA, respectively. The PXRD diffraction peak of pure graphite (Figure 1a) is found around 26° due to the highly layered structure with a 0.34 nm interlayer distance along the (002) orientation. Figure 1b shows the diffraction angle  $2\theta = 10^\circ$ , which is mostly due to the conversion of Gr to GO after the chemical oxidation and exfoliation. At the same time, the 0.34 nm interlayer distance of Gr changed to 0.82 nm, indicating the formation of GO.

Figure 1d shows the PXRD diffraction patterns with a sharp peak of ELA at 9.4, 12.2, 13.5, 17.4, 20.3, 25.0, and 28.1 [2]. The ELA-GO nanocomposite (Figure 1c) shows an amorphous characteristic, with the presence of crystalline peaks of ELA. This result may be due to the presence of free drug in the prepared sample and loaded ELA on the GO carrier. Moreover, the result shows that there is no large change between the diffraction patterns of GO and ELA-GO nanocomposites (the diffraction peak at  $2\theta = 10^\circ$ ), proving that the loading of ELA did not disturb the GO nanocarrier.

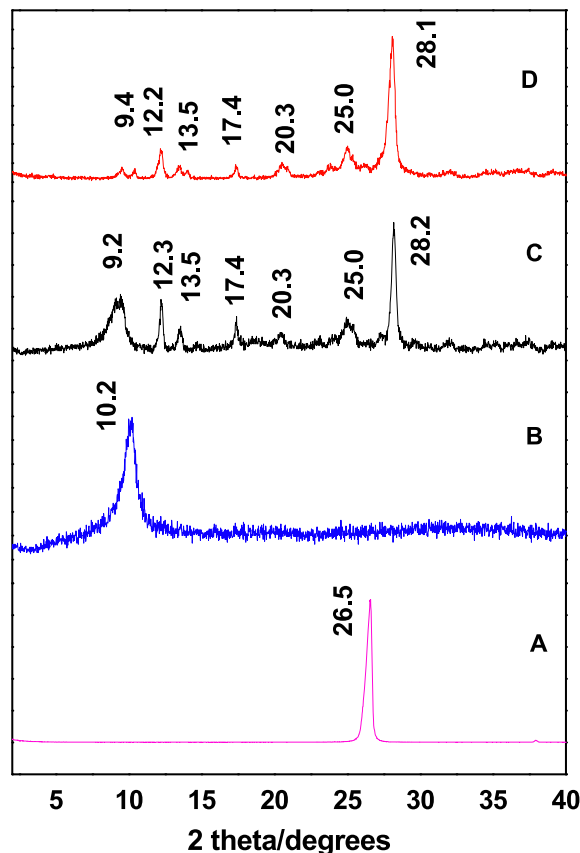


**FIGURE 1** Powder X-ray diffraction (PXRD) patterns of the Gr (a), graphene oxide (GO) (b), ellagic acid (ELA)-graphene oxide (GO) nanocomposite (c) and ELA drug (d)

## 5.2 | Infrared spectroscopy

Figure 2 shows the FTIR spectra analysis of ELA, GO, and ELA-GO. For ELA (Figure 2a), the infrared (IR) characteristic peak of O–H was in the range of 2800–3700  $\text{cm}^{-1}$  [7], and the IR characteristic peak of C=O stretching was at 1697  $\text{cm}^{-1}$  [7,22,23]. The characteristic peaks shown between 1618 and 1510  $\text{cm}^{-1}$  are due to a C=C aromatic ring while characteristic peaks at 1196 and 1059  $\text{cm}^{-1}$  are due to –COO–C ester linkage [7,22,23]. The characteristic peak at 751  $\text{cm}^{-1}$  is due to C–H aromatic bending.

The FTIR spectrum of GO nanosheets is depicted in Figure 2b. The spectrum shows IR characteristic peak of C=O stretching of carboxylic and/or carbonyl moiety functional groups at 1730 and 1618  $\text{cm}^{-1}$  [24] and an IR characteristic peak of C–O stretching vibrations at about 1210 and 1022  $\text{cm}^{-1}$ . This carbonyl group (C=O) in GO would assist the connection of nanoparticles such as gold nanoparticles or protein and DNA through an electrostatic interaction or covalent bond [12,13]. The characteristic peak of ELA at 1333 and 543  $\text{cm}^{-1}$  was clearly observed in Figure 2c, with a slight shift. This suggested that ELA was successfully conjugated on the GO nanosheets.

## 5.3 | The interaction between ellagic acid and graphene oxide in the ellagic acid-graphene oxide nanocomposite

The ELA is a planar phenolic lactone with two deprotonated hydroxyl groups at position eight and/or 8 at pH larger than 5.6 (Figure 3a) [22]. Therefore, the ELA drug was loaded onto the surface of GO by hydrophobic interactions and  $\pi$ – $\pi$  aromatic rings stacking [25]. Two-sandwich structures were opted for in this study, including GO-ELA-GO and ELA-GO-ELA (Figure 3b) [26].

## 5.4 | Determination of the zeta potential ( $\zeta$ )

Figure 4a,b shows the zeta potential ( $\zeta$ ) measurements of the GO and ELA-GO nanocomposite, respectively. From the literature, GO nanosheets are stable in the pH range of 3–12 because their zeta potential is lower than –30 mV, which prevents the GO nanosheets from aggregating through electrostatic repulsion [27]. A GO nanosheets exhibits a zeta potential of about –15 mV, which is due to occurrence of carboxyl groups (COOH) [18]. After loading the ELA drug, the zeta potential ( $\zeta$ ) of the nanocomposite became even more negative with a value of –24 mV, which is appropriate to the larger negatively charged ELA on the surface of GO nanosheets [28].

## 5.5 | Determination of the size distribution properties

Transmission electron microscope imaging was used to characterise the morphology of the GO and ELA-GO

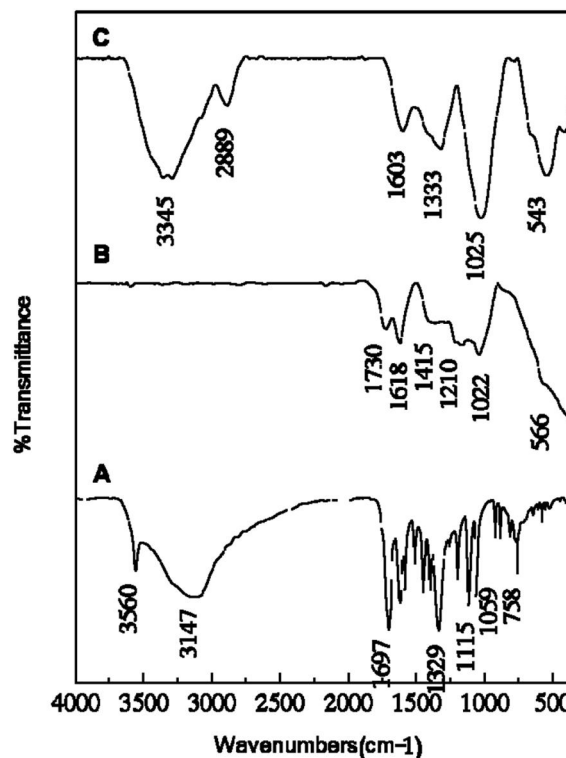


**FIGURE 2** Fourier-transform infrared spectroscopy (FTIR) analysis of the ellagic acid (ELA) (a), graphene oxide (GO) (b), and ELA-GO nanocomposite (c)

nanocomposite. Figure 5a shows a GO nanocarrier multilayered agglomerate [21,29]. The transmission electron microscope images of ELA-GO nanocomposite in Figure 5b also show agglomerate multilayer sheets. The samples of GO and ELA-GO show an average size of 88 and 132 nm, respectively. These average sizes were calculated using Image J software [30].

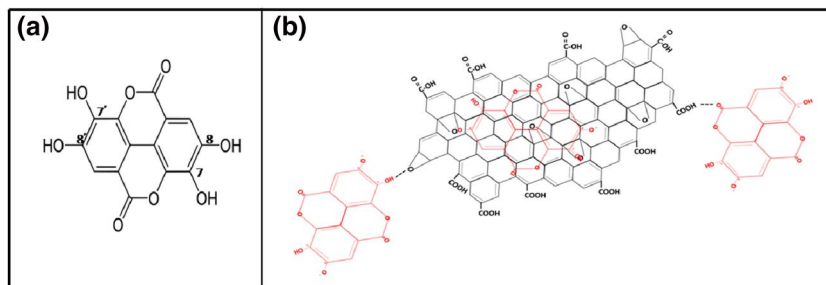
## 5.6 | Scanning electron microscopy analysis

Figure 6a,b shows the SEM images of the GO and ELA-GO nanocomposite at 10,000 $\times$  magnification, respectively. From Figure 6a, it is clear that the sheets are stacked together with exfoliation [31], whereas the morphology of the ELA-GO nanocomposite was loose but porous in Figure 6b [32].

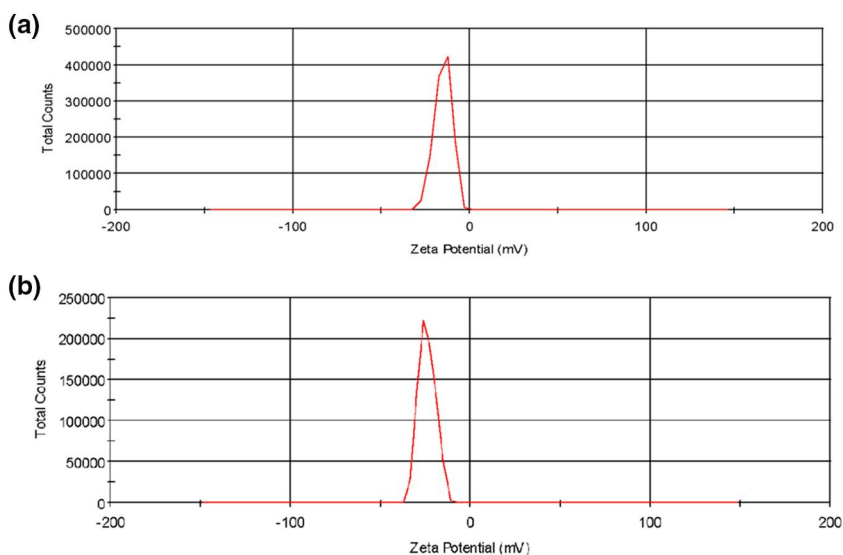
## 5.7 | Thermogravimetric analysis

The TGA thermograms of ELA, GO and ELA-GO nanocomposite are shown in Figure 7. The results from TGA showed that there was a significant mass loss for GO powders. The mass loss percent below 100 $^{\circ}\text{C}$  was related to the evaporation of  $\text{H}_2\text{O}$ , while loss that occurred between 120 $^{\circ}\text{C}$  and 260 $^{\circ}\text{C}$  was related to decomposition of the oxygen functional groups, forming CO and  $\text{CO}_2$  gases [33]. TGA obtained for ELA showed three mass losses; the first mass loss had a value of 8.2% at maximum 112 $^{\circ}\text{C}$  and was due to the removal of

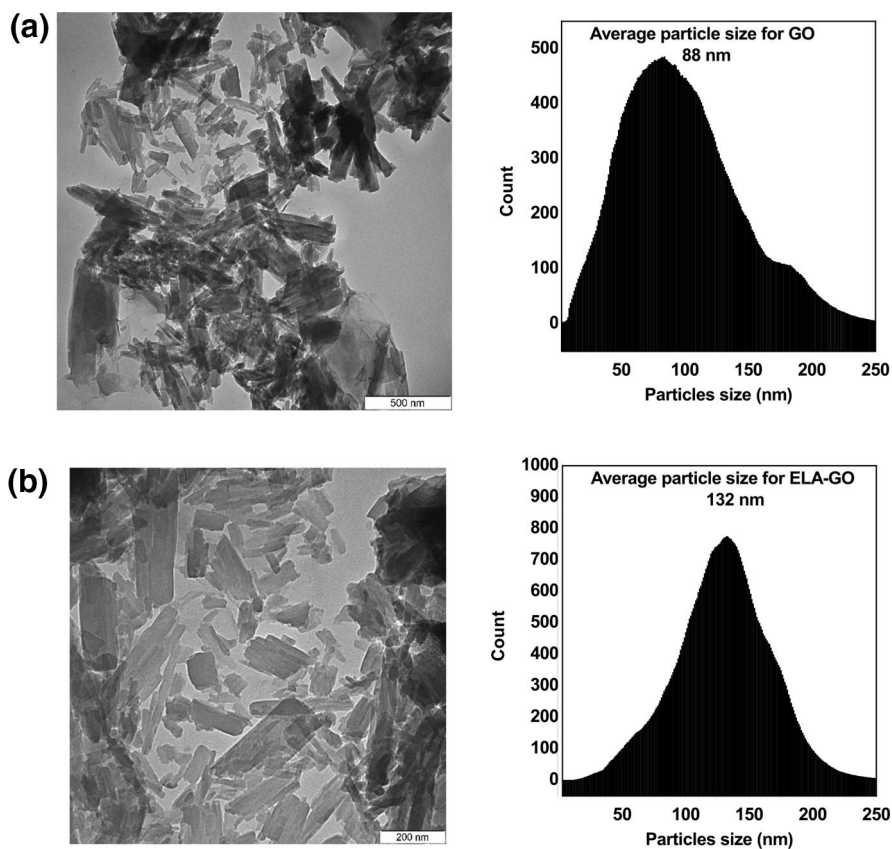
**FIGURE 3** The interaction between ellagic acid (ELA) and graphene oxide (GO) in the ELA-GO nanocomposite



**FIGURE 4** Zeta potential measurements of graphene oxide GO (a) and ellagic acid (ELA)-GO nanocomposite (b)



**FIGURE 5** Transmission electron microscope images of graphene oxide (GO) (a), and ellagic acid (ELA)-GO nanocomposite (b)



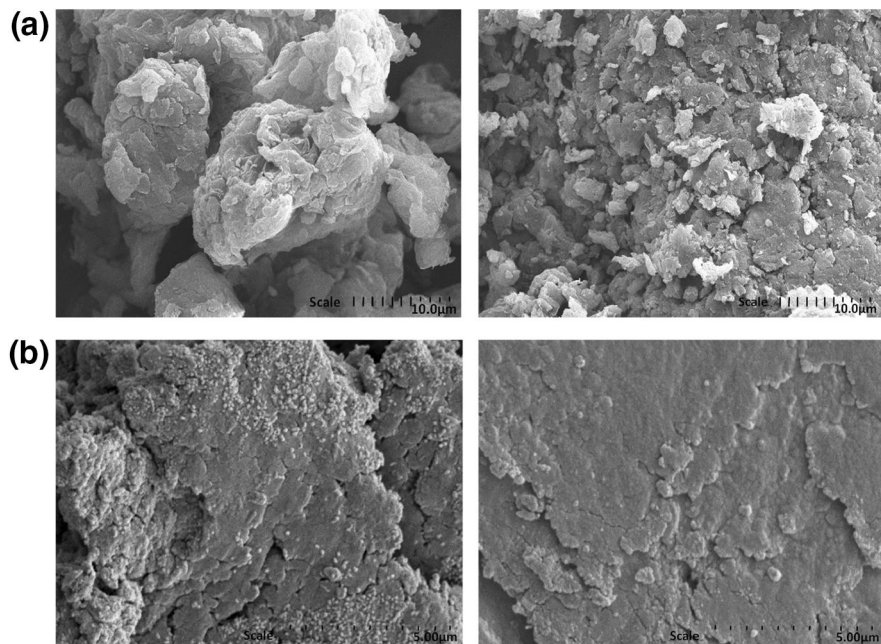


**FIGURE 6** SEM images of graphene oxide (GO) (a), and ellagic acid (ELA)-graphene oxide (GO) nanocomposite (b)

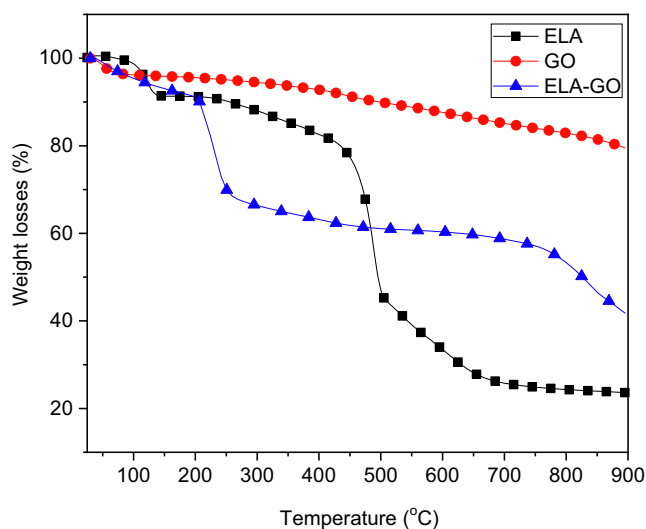


**FIGURE 7** Thermogravimetric analysis (TGA) curves are shown for ellagic acid (ELA), graphene oxide (GO), and ELA-GO nanocomposite

bonded  $H_2O$  with hydrogen bond. The second and third mass losses of ELA occurred at 463 C (39%) and 596 C (17.5%). Because ELA-GO nanocomposite are mainly composed of ELA, their TGA curves are like those of the pristine ELA and have the most significant mass loss between 200°C and 900°C, corresponding to decomposition of ELA. The mass losses for the GO was less than the ELA-GO, thus confirming that the ELA was loaded onto the surface of GO.

## 5.8 | Raman spectroscopy analysis

Raman spectroscopy is a beneficial tool used to describe the structure of GO nanosheets. The Raman spectra of GO and

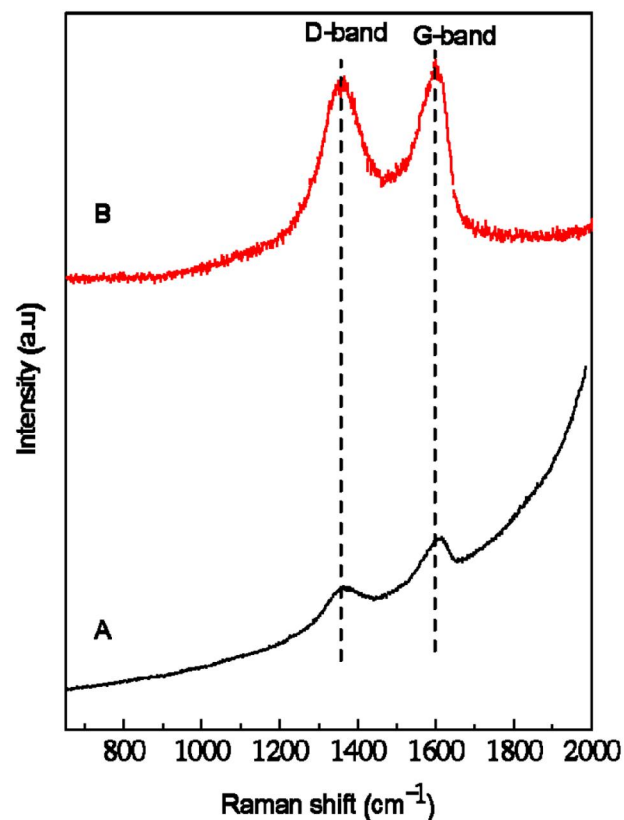


**FIGURE 8** Raman spectra of graphene oxide (GO) (a), and ellagic acid (ELA)-GO nanocomposite (b)

ELA-GO nanocomposite in the spectral region 650–2000  $cm^{-1}$  are presented in Figure 8. In Figure 8a, two fundamental vibrations are shown for G-band at 1607  $cm^{-1}$  and D-band at 1364  $cm^{-1}$ . The G and D bands were due to the first-order scattering of the  $E_{2g}$  mode and  $k$ -point

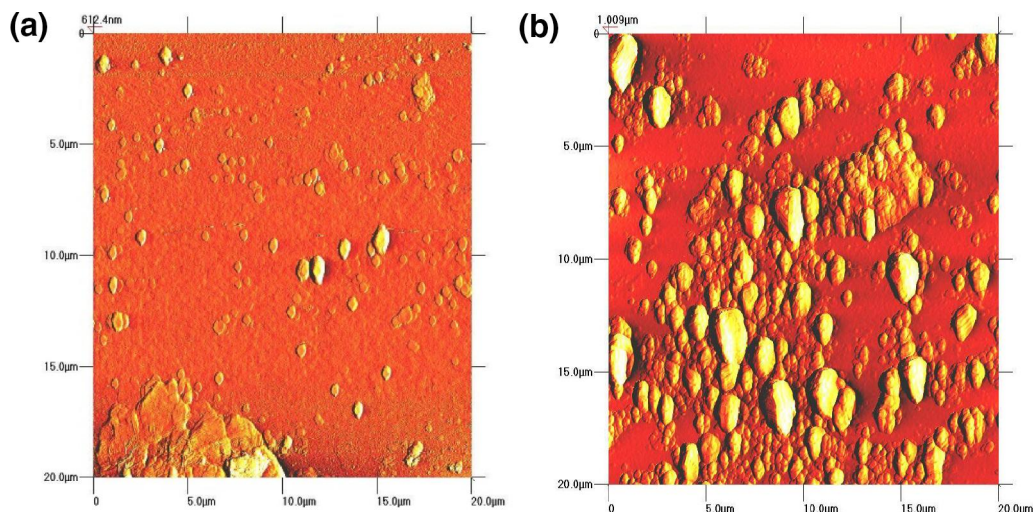


**FIGURE 9** AFM images of GO (a) and ELA-GO nanocomposite (b)

photons of A1g symmetry, respectively [34]. However, for the ELA-GO nanocomposite, the characteristic G and D bands appear at  $1600$  and  $1363\text{ cm}^{-1}$ , respectively. The D/G intensity ratio of the ELA-GO (0.98) increased compared to that of GO (0.76), which indicates that the  $sp^3$  carbon domain in the ELA-GO nanocomposite increased with the loading of GO [35].

### 5.9 | Atomic force microscopy topographic imaging

The vertical distance of GO and ELA-GO is characterised by AFM. Figure 9a shows that the vertical distance of GO is about  $1.3\text{ nm}$  [36], whereas the vertical distance of ELA-GO nanocomposite (Figure 9b) is about  $1.7\text{ nm}$ , which is larger than that of GO. This is due to the adsorption of ELA on both sides of GO [37].

### 5.10 | In vitro release of ellagic acid from ellagic acid-graphene oxide nanocomposite

To study the release actions of ELA from ELA-GO nanocomposite and from physical form, the samples were dispersed in  $0.01\text{ M}$  concentration of phosphate buffer solutions at pH 7.4. A signal was recorded at different time intervals, and the release curve for the physical form of ELA and nanocomposite is shown in Figure 10. This figure shows that ELA is quickly released from the physical form, and release is complete within 100 min in release media. The release rate of ELA from ELA-GO nanocomposite was clearly slower than that from the physical form. This is accredited to the electrostatic attraction between ELA and the different functional groups of GO ( $-\text{OH}$  and  $-\text{COOH}$  groups).

Figure 10 show the release profiles for ELA for the 5000 min. It was found that the release is very quick for the

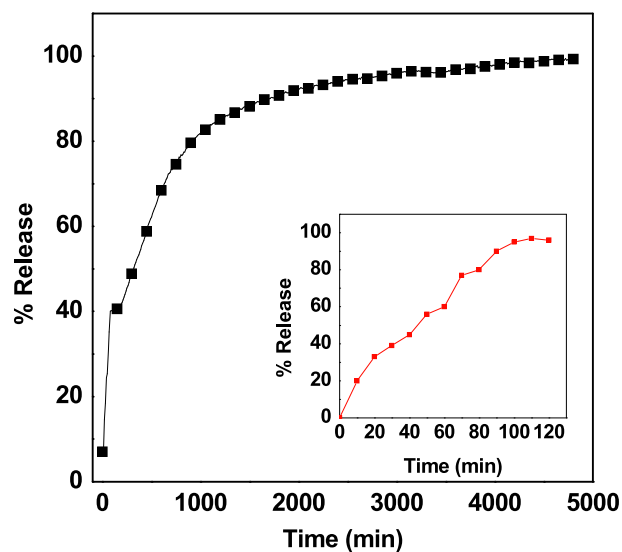


**FIGURE 10** In vitro study of ellagic acid (ELA)-graphene oxide (GO) nanocomposite

first 50 min with 40% release at pH 7.4. This occurrence is most probably due to the 'burst effect' [38], which occurs due to the presence of free ELA in the sample which appeared in the PXRD pattern of the nanocomposite in Figure 1c. After the burst stage, a slower one followed, with a release value of 98% after 4850 min. This result indicates that ELA-GO nanocomposite has potential as a controlled-release formulation of drugs.

The successful formation of ELA-GO nanocomposite was further confirmed by UV-Vis release study. The ELA loading percentage in the nanocomposite was analysed and showed that the value was 30%. The controlled release of ELA from the ELA-GO nanocomposite was performed in  $0.01\text{ M}$  concentration of sodium saline solution (Figure 10). The first burst release occurred at 50 min due to the presence of free ELA in the sample which appeared in Figure 1c. The ELA was released

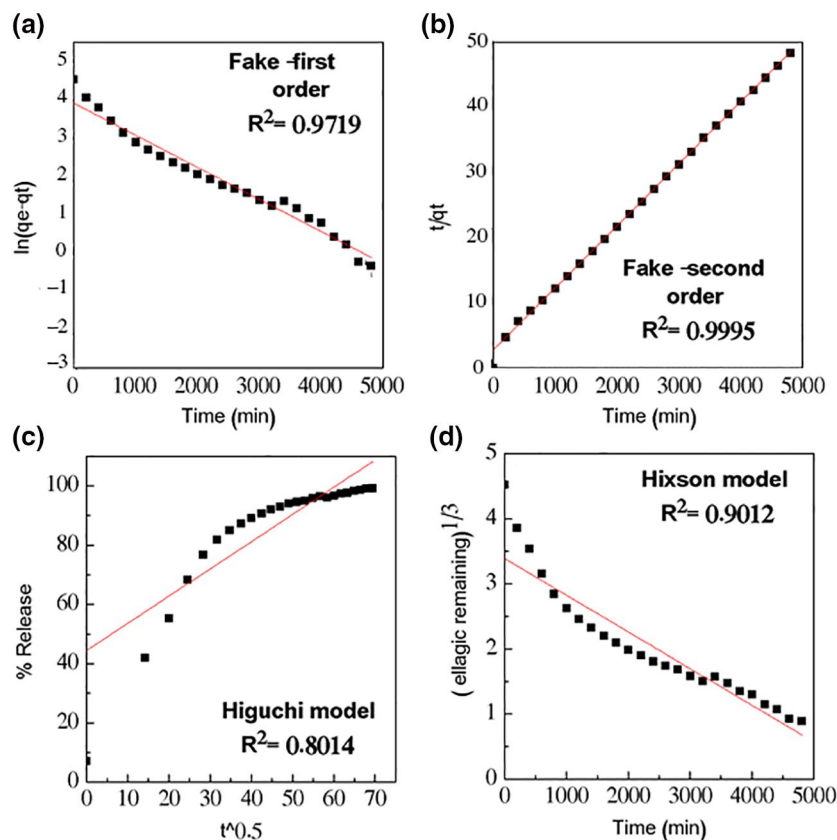


**FIGURE 11** ellagic acid (ELA) release from ELA-graphene oxide (GO) nanocomposite data fitting

very slowly from GO with a 98% value after 4850 min [Figure 10]. This slow release was due to the hydrogen-bonding interaction between  $-OH$  groups in ELA and the  $-COOH$  groups on GO [25,39].

The release rate of ELA from ELA-GO nanocomposite is mostly due to the swelling-diffusion mechanism. The d-spacing can be described as the distance between planes of atoms that can be collected by an XRD instrument [40]. The d-spacing of dry GO initially soaked in water was 0.76 nm. As the GO remained in water for a longer time, the d-spacing increased and reached 6 to 7 nm at equilibrium. This result indicates a swelling of GO in aqueous solution [41]. From the literature, the cefadroxel was diffused from GO nanocomposites due to the exponent diffusion type value ( $n$ ) which is between 0.5 and 1 [42]. According to this result, after the swelling process of GO, the diffusion mechanism of ELA at pH 7.4 occurs easily.

### 5.11 | Drug release kinetics of ellagic acid

ELA release kinetics from the ELA-GO nanocomposite is illustrated in Figure 11. In addition, the regression coefficient ( $R^2$ ) values for ELA are tabulated in Table 1. The model that gave higher  $R^2$  values was considered a best fit model. Based on the  $R^2$  values, it was also observed that the release of ELA from ELA-GO nanocomposite followed the fake-second-order kinetic model (Figure 11) [43].

### 5.12 | Cytotoxicity studies

The cytotoxicity of ELA-GO nanocomposite was compared to that of free ELA and GO on the B16 cancer cell line. In Figure 12b, only ELA-GO nanocomposite produced a dose-dependent cytotoxic effect on B16 cells after 24-h treatment with an  $IC_{50}$  of 6.16  $\mu\text{g/ml}$ . The cells' viability decreased to about 42.4% at 50  $\mu\text{g/ml}$  using ELA-GO nanocomposite, compared to ELA and GO which showed 83.2% and 63.7% decrease in B16 cells' viability, respectively. In the 3T3 cells (Figure 12a), no cytotoxicity effects at concentrations more than 50  $\mu\text{g/ml}$  were observed, indicating that the ELA-GO nanocomposite is safe to use in drug delivery.

### 5.13 | Antimicrobial studies

The results in Table 2 show that the ELA-GO nanocomposite at all tested concentrations (0.5, 1, and 5 mg/ml) have antibacterial activity towards both Gram positive and Gram negative bacteria in a concentration-dependent manner except for 0.5 mg/ml which did not show activity against *P. aeruginosa*.

The effect of ELA-GO nanocomposite was more evident than ELA alone at the same tested concentration (5 mg/ml). ELA showed antibacterial activity against *P. mirabilis*, *E. coli*, and *K. pneumoniae*, and no activity was shown against Gram positive bacteria and *P. aeruginosa*. The GO (5 mg/ml) and



DMSO did not show any antibacterial activity against all the tested bacteria. From these results, it can be deduced that the preparation of ELA-GO nanocomposite will enhance the

antibacterial activity of ELA against both Gram positive and Gram negative bacteria. Krishnamoorthy reported that the GO exhibited antibacterial activity against Gram positive and negative bacteria by mainly generating reactive oxygen species (ROS) which disturb the bacterial cells [44]. Ochemeng studied the effect of several flavones including ELA against the DNA gyrase activity of *E. coli*, and they found that the effect of ELA was evident [45]. Accordingly, this will highlight the importance of using nanocomposite of antimicrobial agents in order to reduce the required concentration of the active materials that are used as antimicrobials by obtaining high activity with less concentration.

**TABLE 1** The  $R^2$  values collected by fitting the ELA drug release data

Models	Equation	$R^2$
Fake-first order	$\ln(q_e - q_t) = \ln q_e - k_1 t$	0.9719
Fake-second order	$t/q_t = 1/k_2 q_e^2 + t/q_e$	0.9995
Higuchi	$q_t = K_H \sqrt{t}$	0.8014
Hixson-Crowell	$\sqrt[3]{M_0} - \sqrt[3]{q_t} = Kt$	0.9012

Abbreviations: ELA, ellagic acid.

**FIGURE 12** The cytotoxicity profiles for the ellagic acid (ELA), graphene (GO) and ELA-GO nanocomposite after treatment of 3T3 cells (a) and B16 cells (b)

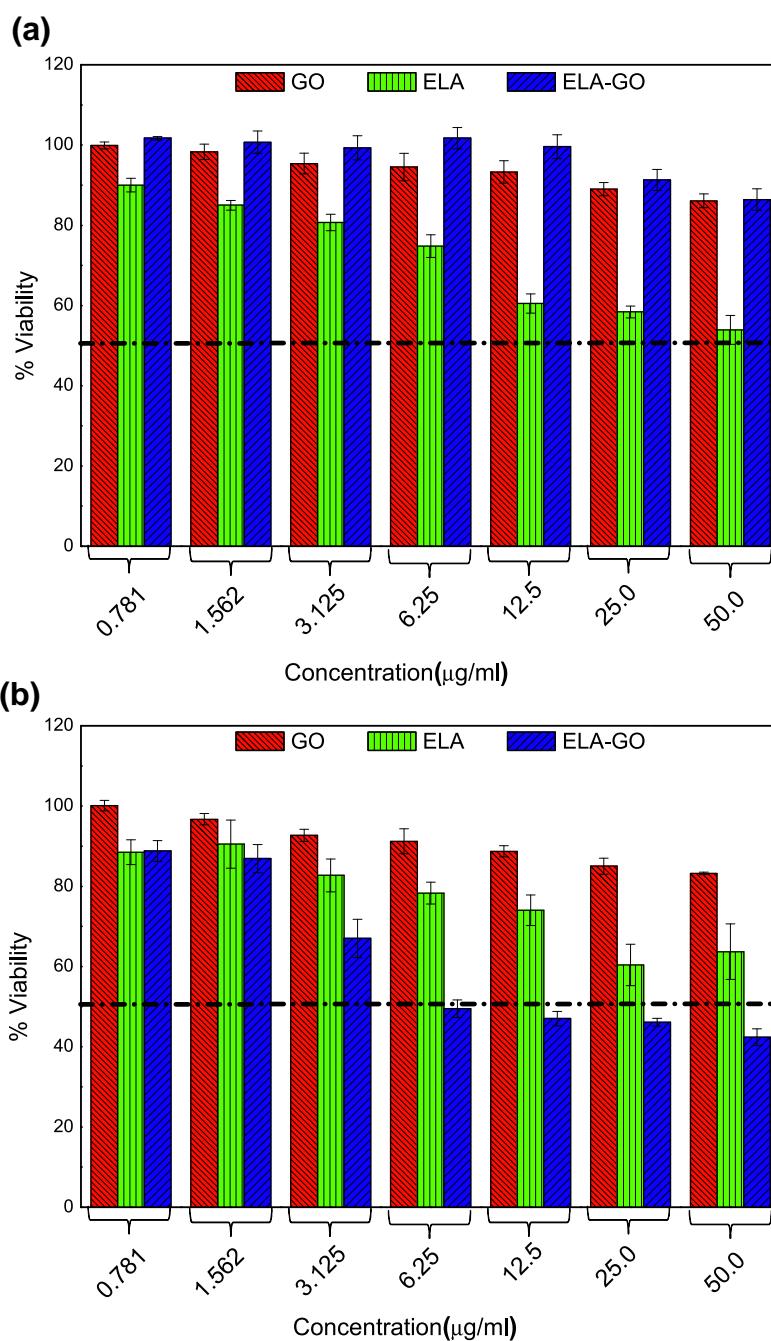


**TABLE 2** Antimicrobial activity of ELA, GO and ELA-GO nanocomposite

Microorganism	Diameter of zone of inhibition (mm)						
	5 mg/ml			1 mg/ml		0.5 mg/ml	
	EA-GO	EA	GO	EA-GO	EA	EA-GO	EA
<i>Proteus mirabilis</i>	3.07 ± 0.089	1.65 ± 0.070	0	2.63 ± 0.044	1.1 ± 0.141	2.53 ± 0.057	0
<i>Escherichia coli</i>	2.77 ± 0.156	1.6 ± 0.141	0	2.43 ± 0.044	1.3 ± 0.141	2.23 ± 0.057	0
<i>Pseudomonas aeruginosa</i>	2.5 ± 0.067	0	0	1.56 ± 0.044	0	0	0
<i>Klebsiella pneumoniae</i>	3.3 ± 0.11	1.5 ± 0.141	0	2.93 ± 0.178	1.15 ± 0.070	2.83 ± 0.152	0
MRSA	2.87 ± 0.11	0	0	2.27 ± 0.156	0	2.07 ± 0.115	0
<i>Staphylococcus aureus</i>	2.97 ± 0.15	0	0	2.33 ± 0.111	0	2.17 ± 0.152	0

Note: The diameter of zone of inhibition for dimethyl sulfoxide (DMSO) was zero.

Abbreviations: ELA, ellagic acid; GO, graphene oxide; MRSA, methicillin-resistant *S. aureus*.

## 6 | CONCLUSION

In conclusion, this study confirmed the successful loading of ELA onto the surface(s) of GO. The nanocomposite was characterised by XRD, FTIR, TGA, TEM, SEM, AFM, and zeta-potential. This nanocomposite could successfully affect B16 cells and lead to tumor cell inhibition with an  $IC_{50}$  of 6.16  $\mu\text{g}/\text{ml}$ . In contrast, the ELA and GO alone did not show any inhibition to the same cells. The release of the ELA from ELA-GO nanocomposite followed fake-second order kinetic model. In addition, The of ELA-GO nanocomposite was more evident than ELA alone at the same tested concentration (5 mg/ml).

## ACKNOWLEDGEMENTS

Dr. Samer Hasan would like to thank the Faculty of Pharmacy at Isra University, and University Putra Malaysia under grant number (9,443,100 NANOMITE) for providing funding for this research.

## ORCID

Samer Hasan Hussein-Al-Ali  <https://orcid.org/0000-0002-8760-6069>

## REFERENCES

- Strati, A., et al.: Effect of ellagic acid on the expression of human telomerase reverse transcriptase (hTERT)  $\alpha + \beta +$  transcript in estrogen receptor-positive MCF-7 breast cancer cells. *Clin Biochem.* 42(13-14), 1358–1362 (2009)
- Kim, S., et al.: Development of chitosan–ellagic acid films as a local drug delivery system to induce apoptotic death of human melanoma cells. *J. Biomed. Mater. Res. B Appl. Biomater.* 90(1), 145–155 (2009)
- Hussein, M.Z., et al.: Development of antiproliferative nanohybrid compound with controlled release property using ellagic acid as the active agent. *Int. J. Nanomed.* 6, 1373 (2011)
- Hussein-Al-Ali, S.H., et al.: The in vitro therapeutic activity of ellagic acid-alginate-silver nanoparticles on breast cancer cells (MCF-7) and normal fibroblast cells (3T3). *Sci. Adv. Mater.* 8(3), 545–553 (2016)
- Dubey, A., et al.: Investigation of the biological and anti-cancer properties of ellagic acid-encapsulated nano-sized metalla-cages. *Int. J. Nanomed.* 10, 227 (2015)
- Bala, I., et al.: Sustained release nanoparticulate formulation containing antioxidant-ellagic acid as potential prophylaxis system for oral administration. *J. Drug Target.* 14(1), 27–34 (2006)
- Gopalakrishnan, L., et al.: Ellagic acid encapsulated chitosan nanoparticles as anti-hemorrhagic agent. *Carbohydr Polym.* 111, 215–221 (2014)
- Ardestani, M.S., et al.: Synthesis and characterization of novel  $^{99m}\text{Tc}$ -DGC nano-complexes for improvement of heart diagnostic. *Bioorg. Chem.* 96, 103572 (2020)
- Mohammadzadeh, P., et al.: PEG-Citrate dendrimer second generation: is this a good carrier for imaging agents in vitro and in vivo? *IET Nanobiotechnol.* 13(6), 560–564 (2019)
- Mortazavi-Derazkola, S., Reza Naimi-Jamal, M., Masoumeh Ghoreishi, S.: Synthesis, characterization, and atenolol delivery application of functionalized mesoporous hydroxyapatite nanoparticles prepared by microwave-assisted co-precipitation method. *Curr. Drug Deliv.* 13(7), 1123–1129 (2016)
- Zhou, N., et al.: Coprecipitation synthesis of a green Co-doped wurtzite structure high near-infrared reflective pigments using ammonia as precipitant. *J. Alloys Compd.* 820, 153183 (2020)
- Yang, Q., et al.: Fabrication of high-concentration and stable aqueous suspensions of graphene nanosheets by noncovalent functionalization with lignin and cellulose derivatives. *J. Phys. Chem. C.* 114(9), 3811–3816 (2010)
- Zhang, S., et al.: In vitro and in vivo behaviors of dextran functionalized graphene. *Carbon.* 49(12), 4040–4049 (2011)
- Khojasteh, H., et al.: Economic procedure for facile and eco-friendly reduction of graphene oxide by plant extracts; a comparison and property investigation. *J. Clean Prod.* 229, 1139–1147 (2019)
- Wang, S., et al.: Band-like transport in surface-functionalized highly solution-processable graphene nanosheets. *Adv. Mater.* 20(18), 3440–3446 (2008)
- Stankovich, S., et al.: Graphene-based composite materials. *Nature.* 442(7100), 282–286 (2006)
- Xu, Y., et al.: A graphene hybrid material covalently functionalized with porphyrin: synthesis and optical limiting property. *Adv. Mater.* 21(12), 1275–1279 (2009)
- Wu, S., et al.: Adsorption properties of doxorubicin hydrochloride onto graphene oxide: equilibrium, kinetic and thermodynamic studies. *Materials.* 6(5), 2026–2042 (2013)
- Zhu, X., et al.: Functionalized graphene oxide-based thermosensitive hydrogel for near-infrared chemo-photothermal therapy on tumor. *J. Biomater. Appl.* 30(8), 1230–1241 (2016)
- Marcano, D.C., et al.: Improved synthesis of graphene oxide. *ACS Nano.* 4(8), 4806–4814 (2010)
- Dorniani, D., et al.: Graphene oxide-gallic acid nanodelivery system for cancer therapy. *Nano. Res. Lett.* 11(1), 491 (2016)
- Hasegawa, M., et al.: Deprotonation processes of ellagic acid in solution and solid states. *Monatsh. Chem./Chem. Mon.* 134(6), 811–821 (2003)
- Bindra, R., Satti, N., Suri, O.: Isolation and structures of ellagic acid derivatives from *Euphorbia acaulis*. *Phytochemistry.* 27(7), 2313–2315 (1988)

24. Schwenzer, B., et al.: Spectroscopic study of graphene oxide membranes exposed to ultraviolet light. *J. Phys. Chem. C.* 120(23), 12559–12567 (2016)
25. Yang, X., et al.: Multi-functionalized graphene oxide based anticancer drug-carrier with dual-targeting function and pH-sensitivity. *J. Mater. Chem.* 21(10), 3448–3454 (2011)
26. Huang, P., et al.: Folic acid-conjugated graphene oxide loaded with photosensitizers for targeting photodynamic therapy. *Theranostics.* 1, 240 (2011)
27. Chen, J.-T., et al.: Tuning nanostructure of graphene oxide/poly-electrolyte LbL assemblies by controlling pH of GO suspension to fabricate transparent and super gas barrier films. *Nanoscale.* 5(19), 9081–9088 (2013)
28. Ghosh, D., et al.: A novel graphene oxide-para amino benzoic acid nanosheet as effective drug delivery system to treat drug resistant bacteria. *Int. J. Pharm. Sci. Drug Res.* 2(89), 127–133 (2010)
29. Verma, S., et al.: Graphene oxide: an efficient and reusable carbocatalyst for aza-Michael addition of amines to activated alkenes. *Chem. Commun.* 47(47), 12673–12675 (2011)
30. Igathinathane, C., et al.: Shape identification and particles size distribution from basic shape parameters using ImageJ. *Comput. Electron. Agric.* 63(2), 168–182 (2008)
31. Paulchamy, B., Arthi, G., Lignesh, B.: A simple approach to stepwise synthesis of graphene oxide nanomaterial. *J. Nanomed. Nanotechnol.* 6(1), 1 (2015)
32. Zhu, X., et al.: Functionalized graphene oxide-based thermosensitive hydrogel for magnetic hyperthermia therapy on tumors. *Nanotechnology.* 26(36), 365103 (2015)
33. Stankovich, S., et al.: Synthesis of graphene-based nanosheets via chemical reduction of exfoliated graphite oxide. *Carbon.* 45(7), 1558–1565 (2007)
34. Lin, Z., et al.: Solvent-assisted thermal reduction of graphite oxide. *J. Phys. Chem. C.* 114(35), 14819–14825 (2010)
35. Kudin, K.N., et al.: Raman spectra of graphite oxide and functionalized graphene sheets. *Nano Lett.* 8(1), 36–41 (2008)
36. Zhu, C., et al.: Reducing sugar: new functional molecules for the green synthesis of graphene nanosheets. *ACS Nano.* 4(4), 2429–2437 (2010)
37. Huang, Y., Liu, P., Wang, L.: Production of stable dispersions of reduced graphene oxide using indole as a reduction agent. *Nano.* 8(02), 1350017 (2013)
38. Arizaga, G.G.C., et al.: Intercalation of an oxalatoxonobate complex into layered double hydroxide and layered zinc hydroxide nitrate. *J. Colloid. Interface Sci.* 330(2), 352–358 (2009)
39. Yang, X., et al.: High-efficiency loading and controlled release of doxorubicin hydrochloride on graphene oxide. *J. Phys. Chem. C.* 112(45), 17554–17558 (2008)
40. Bourdillon, A.: The measurement of impact parameters by crystallographic orientation effects in electron scattering. *Philos. Mag. A.* 50(6), 839–848 (1984)
41. Zheng, S., et al.: Swelling of graphene oxide membranes in aqueous solution: characterization of interlayer spacing and insight into water transport mechanisms. *ACS Nano.* 11(6), 6440–6450 (2017)
42. Raafat, A.I., Ali, A.E.-H.: pH-controlled drug release of radiation synthesized graphene oxide/(acrylic acid-co-sodium alginate) interpenetrating network. *Polym. Bull.* 74(6), 2045–2062 (2017)
43. Dash, S., et al.: Kinetic modeling on drug release from controlled drug delivery systems. *Acta Pol. Pharm.* 67(3), 217–223 (2010)
44. Krishnamoorthy, K., et al.: Antibacterial activity of graphene oxide nanosheets. *Sci. Adv. Mater.* 4(11), 1111–1117 (2012)
45. Ohemeng, K., et al.: DNA gyrase inhibitory and antibacterial activity of some flavones (1). *Bioorg. Med. Chem. Lett.* 3(2), 225–230 (1993)

**How to cite this article:** Hussein-Al-Ali SH, Abudoleh SM, Hussein MZ, Bullo S, Palanisamy A. Graphene oxide-ellagic acid nanocomposite as effective anticancer and antimicrobial agent. *IET Nanobiotechnol.* 2021;15:79–89. <https://doi.org/10.1049/nbt2.12009>